Probing Halogen Bonds with Solid–State NMR Spectroscopy. Observation and Interpretation of J(77Se, 31P) Coupling in Halogen-Bonded P=Se●●●I Motifs

Journal:	*CrystEngComm*
Manuscript ID:	CE-ART-02-2014-000345.R1
Article Type:	Paper
Date Submitted by the Author:	14-Mar-2014
Complete List of Authors:	Viger-Gravel, Jasmine; University of Ottawa, Chemistry Meyer, Julia; University of Ottawa, Department of Chemistry Korobkov, Ilia; University of Ottawa, Department of Chemistry Bryce, David L. ; University of Ottawa, Department of Chemistry

Probing Halogen Bonds with Solid-State NMR Spectroscopy. Observation and Interpretation of $J(^{77}\text{Se}, {}^{31}\text{P})$ Coupling in Halogen-Bonded P=Se···I Motifs

Jasmine Viger-Gravel, Julia E. Meyer, Ilia Korobkov, and David L. Bryce*

*Author to whom correspondence is to be addressed.

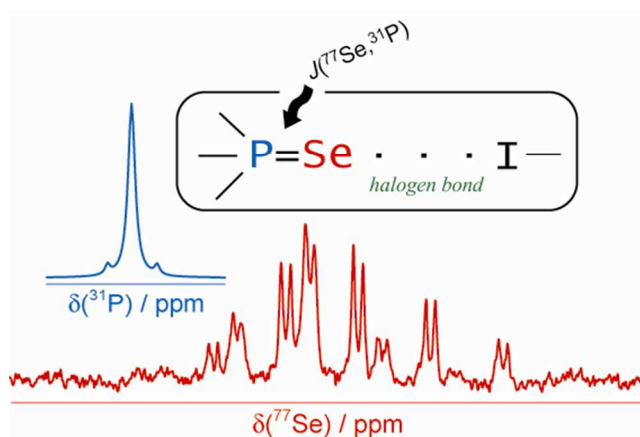Department of Chemistry and Center for Catalysis Research and Innovation

University of Ottawa

10 Marie Curie Private

Ottawa, Ontario, Canada K1N 6N5

Tel.: +1 613 562 5800 ext. 2018; Fax: +1 613 562 5170

E-mail: dbryce@uottawa.ca

Graphical abstract

One sentence summary

Intra-halogen bond J couplings measured via NMR spectroscopy and interpreted using natural

localized molecular orbitals offer novel insights into this class of non-covalent interaction.

Abstract

Halogen bonds constitute an important and topical class of non-covalent interaction. We report a combined X-ray diffraction, multinuclear (^{77}Se, ^{31}P, ^{13}C) solid-state magnetic resonance, and computational study of a series of crystalline triphenylphosphine selenide-iodoperfluorobenzene complexes which feature P=Se···I-C halogen bonds. Selenium-77 chemical shifts increase due to halogen bonding with iodine and correlate with the P=Se distance, which in turn correlates with the strength of the halogen bond. $J(^{77}\text{Se}, ^{31}\text{P})$ coupling constants increase as the halogen bond weakens. This observation is understood via a natural localized molecular orbital (NLMO) DFT approach which shows that contributions from the selenium lone pair orbital tend to dominate both the magnitude and trends in $J(^{77}\text{Se}, ^{31}\text{P})$, with the selenium-phosphorus bonding orbital being the second-largest contributor. This work suggests that J couplings measured via NMR spectroscopy may play an important role in the characterization of halogen bonds, in clear analogy with its role in the characterization of hydrogen bonds.

Introduction

Halogen bonds (R-X···Y-Z) are the result of a non-covalent interaction between an electron donor (Y) and a region of positive electrostatic potential on a halogen (X) typically bound to an electron-withdrawing group (R).[1,2] Such interactions have long been known,[3] but have been the focus of increased interest in recent years.[4,5,6,7,8,9,10,11] Important fundamental studies have described the nature of the interaction in terms of electrostatic and charge-transfer contributions,[12,13,14,15] and the σ-hole concept has become a useful paradigm.[14,16,17,18] The strength of the halogen bond ranges from about 1 to 43 kcal mol^{-1} and they are strongly directional.[12,16] Recent applications describe the role of halogen bonding in nucleic acid structure,[19,20] anion recognition,[21,22,23] selective binding and release of small molecules,[24,25] gelation,[26] and supramolecular chemistry.[5,27,28]

The similarities, differences, and interplay between halogen bonds and hydrogen bonds have been discussed.[29,30,31,32] In this context, we consider the impact which NMR spectroscopy has had on the characterization and understanding of hydrogen bonds in solution and in the solid state and compare this to the current situation for halogen bonds. Carlsson et al. have elegantly probed the symmetry of halogen bonds in solution using NMR chemical shifts.[33] Yan et al. have recently studied the possible application of σ-hole···Cl$^-$ bonds in separation science using ^{19}F NMR titration experiments in solution.[34] We have recently reported solid-state NMR (SSNMR) studies of halogen-bonded complexes and demonstrated the relationships between various NMR observables and the halogen bond geometry and environment.[35,36,37,38] For instance, ^{13}C chemical shifts of the ipso <u>C</u>-I carbon in diiodoperfluorobenzene-halide complexes exhibiting halogen bonds were shown to be sensitive to the C-I bond length, which in turn is a measure of the extent of halogen bonding in the C-I···X$^-$ motif.[36] Chlorine-35/37, bromine-79/81, and

iodine-127 SSNMR spectroscopies of halogen-bonded anions have revealed the sensitivity of the nuclear quadrupolar coupling tensors to the halogen bond environment.[37,38]

The study of hydrogen bonds (e.g., N-H···O=C in proteins) by NMR spectroscopy took a quantum leap forward with the successful measurement and interpretation of indirect nuclear spin-spin (J) couplings across and within such bonds, in solution and in the solid state.[39, 40, 41, 42] For example, Limbach and co-workers have examined such couplings experimentally and computationally in small molecules.[43,44] J couplings have also been measured in van der Waals' complexes[45] and have been used to characterize CH-π interactions.[46]

J couplings are present in principle between the various nuclei involved in a halogen bond. To our knowledge, however, J coupling constants have not been measured experimentally for halogen bonds. Computed J coupling constants for model systems in the gas phase have been reported, and these suggest that non-negligible one-bond and two-bond couplings are possible and that there is a dependence on the local geometry.[47] We report here a multinuclear SSNMR study of phosphine selenide-iodofluorobenzene complexes exhibiting P=Se···I halogen bonds. J couplings measured between ^{31}P and ^{77}Se (both spin-1/2 nuclides) are shown to be sensitive to the presence and geometry of the halogen bond between the P=Se and I-C moieties. ^{77}Se and ^{31}P chemical shift tensors are also measured experimentally and interpreted in relation to halogen bonding. Related work has demonstrated the sensitivity of $J(^{77}$Se,^{31}P) coupling to selenium-cadmium interactions in solutions containing phosphine selenides and cadmium complexes.[48,49] Our data are interpreted in the context of single-crystal and powder X-ray diffraction data and density functional theory (DFT) calculations. A natural localized molecular orbital (NLMO)[50] DFT analysis of the $J(^{77}$Se, ^{31}P) coupling constants provides insight into the connection between the experimental observables and the electronic structure. Such analyses

have been applied to study magnetic shielding tensors, electric field gradient tensors, and J couplings in a variety of systems.[51,52,53,54]

Results and Discussion

The Structures of (Ph$_3$PSe)(o-DITFB) and (Ph$_3$PSe)(sym-TITFB)

Co-crystallization of triphenylphosphine selenide (Ph$_3$PSe) and iodobenzene derivatives (*o*- or *p*-C$_6$F$_4$I$_2$ and *sym*-C$_6$F$_3$I$_3$ which are also referred to as DITFB and TITFB, respectively) yielded two novel co-crystals exhibiting halogen bonds, (Ph$_3$PSe)(*o*-DITFB) (**2**) and (Ph$_3$PSe)(*sym*-TITFB) (**3**), and (Ph$_3$PSe)(*p*-DITFB) (**1**) which was previously reported by Arman et al.[70] The relevant halogen bond distances, $d_{I \cdots Se}$, angles, $\theta_{C-I \cdots Se}$, and I$\cdots$Se$\cdots$I angles ($\theta_{I \cdots Se \cdots I}$), as well as carbon-iodine bond lengths (d_{I-C}), phosphorus-selenium bond lengths ($d_{P=Se}$), and P=Se$\cdots$I angles ($\theta_{P=Se \cdots I}$) are given in Table 1. The normalized distance parameter ($R_{XB} = d_{X \cdots Y}$ /Σd_{VdW}), which is one measure of the extent of halogen bonding, is equal to the ratio of the distance between the halogen (i.e., I) and the electron donor (i.e., Se) to the sum of their van der Waals radii (1.98 Å for I and 2.00 Å for Se).[55] Summarized in Table 2 are the crystallographic data for compounds **2** and **3**.

The X-ray crystal structure of **1** was verified to match that reported previously.[70] The halogen bond environments in **1** may be described as follows: there are two different selenium sites and both engage in halogen bonding with iodine. Interactions at one of the sites (labelled site 2 in Figure 1) result in infinite chains along the *a* axis involving one halogen bond acceptor (i.e., Se) and two halogen bond donors from different *p*-DITFB molecules. Selenium atoms in

the other distinct site (labelled site 1 in Figure 1) interact with one iodine atom and the result is discrete halogen-bonded entities rather than infinite chains.

One polymorph of compound **2** has been previously reported;[70] however, we report a different polymorph here which crystallizes in the P$2_1/n$ space group (Table 2). The polymorph synthesized in this work features discrete halogen-bonded entities; the selenium atom forms short contacts with two iodine atoms (R_{XB} = 0.85 and 0.90) from different arene molecules with a I···Se···I angle of 138.8°. The C—I···Se angles are nearly linear (175.2° and 174.7°). The local structural motif is shown in Figure 1. The extended crystal network is shown in Figure S1 (Supplementary Information, SI).

Compound **3** crystallizes in the P$2_1/n$ space group. This halogen-bonded compound has two crystallographically distinct P=Se environments (see Figure 1). The first selenium atom interacts with a single iodine atom (R_{XB} = 0.89; $\theta_{C—I···Se}$ = 166.8°), resulting in discrete entities in the crystal lattice (see Figure S2, SI). The second crystallographically distinct type of selenium atom is surrounded by three iodine atoms from different *sym*-TITFB molecules as depicted in Figure 1. The values of R_{XB} for each of the three Se···I contacts are 0.88, 0.91, and 0.99, respectively. This indicates that the third contact hardly constitutes a halogen bond (i.e., an R_{XB} value of 1 implies that the atoms in question are no closer than the sum of their van der Waals' radii). The two iodine atoms involved in halogen bonding with Se form a I···Se···I angle of 118.6°. These interactions at the second selenium site result in polymeric zigzag chains along the *b* axis (Figure S2).

Initial Characterization

To verify the phase purity of **1**, **2**, and **3** upon grinding of the crystals for solid-state NMR spectroscopy, we performed powder X-ray diffraction (PXRD) experiments which provided diffractograms in good agreement with those predicted from the single-crystal X-ray crystal structures (see Figure S3, SI). ^{13}C cross-polarization magic-angle spinning (CP/MAS) SSNMR spectra (see Figure S4, SI) also suggest the formation of halogen bonds in the structures. As expected, the chemical shifts of the carbon atoms covalently bonded to iodine (C-I) are quite shielded due to the relativistic spin-orbit-induced 'heavy-atom light-atom' (HALA) effect caused by the covalently bonded iodine.[56] The average values for **1**, **2**, and **3** are 73.4, 97.6, and 65.3 ppm, respectively. These chemical shifts differ from those of the parent iodobenzenes (e.g., 76.5 ppm for solid *p*-DITFB[36] and 64.0 ppm for *sym*-TITFB[57] (in chloroform-*d*)). All three compounds have more than one crystallographically distinct C-I site (four for **1**, two for **2**, and five for **3**) but only one broad ^{13}C NMR peak is observed in each case. This is due to spectral overlap and possible line broadening due to the nearby iodine and fluorine nuclei. For example, a residual ^{127}I-^{13}C dipolar coupling of -2.4 kHz at 9.4 T is expected on the basis of a one-bond ^{127}I-^{13}C dipolar coupling constant of 657 Hz and a typical $C_Q(^{127}I)$ of 1000 MHz.

^{31}P and ^{77}Se SSNMR spectroscopy of halogen-bonded compounds

The ^{31}P and ^{77}Se CP/MAS SSNMR spectra of triphenylphosphine selenide have been thoroughly investigated by Demko et al.[58] as well as Grossmann et al.[59] The latter study was performed on a Ph$_3$PSe sample which was 70% isotopically enriched in ^{77}Se, resulting in spectra with excellent signal-to-noise. The ^{31}P and ^{77}Se data from these previous studies are used for comparison with the data obtained for halogen-bonded compounds **1**, **2**, and **3** (see Tables 3 and 4). All compounds in the present study were investigated at natural isotopic abundance.

Presented in Figure 2 are the ^{31}P CP/MAS NMR spectra of compounds **1**, **2**, and **3** obtained in an applied magnetic field of 9.4 T. Analogous data obtained at 11.75 T are provided in the Supplementary Information. The isotropic chemical shifts, span, and skew are presented in Table 3. The total range of chemical shifts observed is from 31.85 ppm in **2** to 41.90 ppm in site 2 of Ph$_3$PSe. Two crystallographically distinct phosphorus sites are expected for **1**; however, only one is resolved in the ^{31}P SSNMR spectrum. It is noted that there is a small but consistent decrease in the ^{31}P chemical shifts in the halogen-bonded compounds relative to both sites in Ph$_3$PSe where halogen bonding is absent. Similarly, the ^{31}P chemical shift tensor spans are smaller in the halogen-bonded complexes (ranging from 112 to 134 ppm) relative to both sites in Ph$_3$PSe (144 and 166 ppm). The span (Ω) is a measure of the degree of anisotropy of the chemical shift tensor and a smaller span reflects a small change in the electronic structure of the P=Se bond in the halogen-bonded complexes.

Also shown in Figure 2 are expansions of the centreband where the *J* coupling between ^{31}P and ^{77}Se may be observed in the satellite peaks (note that the natural abundance of ^{77}Se is 7.63%). The values obtained from these spectra are consistent with those obtained from the corresponding ^{77}Se CP/MAS NMR spectra of the same compounds (see Table 4); however, analysis of the latter spectra (*vide infra*) allows for improved precision since the effects of the coupling are clearly seen in the main peaks rather than in low-intensity satellites which partially overlap with the main peaks.

Shown in Figures 3, 4, and 5 are the ^{77}Se CP/MAS SSNMR spectra of **1**, **2**, and **3** recorded at 9.4 T with two different spinning frequencies. Spectral fitting at two MAS frequencies, as well as at more than one applied magnetic field strength (at least 9.4 T and 11.75 T), allows for the measurement of the isotropic $J(^{77}$Se, ^{31}P$)$ coupling and the ^{77}Se chemical shift

tensor magnitude. Simulations also included the direct dipolar coupling between ^{77}Se and ^{31}P ($R_{DD} = (\mu_0/4\pi)(\gamma_{77Se}\gamma_{31P}\hbar/2\pi)<r^{-3}>$ where r is the distance between the spins), as well as contributions from the anisotropic part of the **J** tensor (ΔJ).[60,61,62] The ^{77}Se CS tensor parameters and J coupling values are presented in Table 4 and were obtained by simultaneously modeling the NMR spectra obtained at both MAS frequencies and in both applied magnetic fields. For **2**, three magnetic fields were used to model the NMR spectra (see Figure S6 for ^{77}Se CP/MAS SSNMR spectra acquired at 11.75 and 21.1 T). Fitting was done in a manual iterative fashion, by cycling between the various spectra until a self-consistent set of parameters was determined. Error estimates were obtained through this process as well. Errors in $J(^{77}$Se, ^{31}P$)$ are larger than those which would be obtained from signal-to-noise or digital resolution estimates on a single spectrum.

Such spectra were difficult to acquire due to the presence of the nearby fluorines and protons (dipolar coupling), long ^{1}H relaxation times, as well as the halogen-bonded iodines (residual dipolar coupling), which resulted in broad lines particularly in **2**. For all compounds, the $J(^{77}$Se, ^{31}P$)$ coupling is resolved and ranges between -626(2) Hz for (Ph$_3$PSe)(o-DITFB) and -725(25) Hz for (Ph$_3$PSe)(p-DITFB). It is important to note here that the assignments of the two different $J(^{77}$Se, ^{31}P$)$ coupling values to their different crystallographic P=Se sites in a particular compound were determined independently from the ZORA-DFT calculations (*vide infra*).

R_{DD} and ΔJ cannot be separated in an NMR experiment; an effective direct dipolar coupling describes the effects of both: $R_{eff} = R_{DD} - \Delta J/3$. For spectral simulation, the values used for R_{DD} were calculated from the X-ray crystal structures (see Table 1) and ΔJ values were estimated at 900 Hz, which is the approximate value observed for various organophosphine

selenides.[58]   The R_{eff} values shown here were fixed for spectral simulations rather than determined from the experimental MAS spectra because simulations of the latter were not sensitive enough to the value of ΔJ to be able to determine values with high precision. The [77]Se-^{31}P dipolar and [77]Se chemical shift tensors were set to be coincident in all spectral simulations (δ_{33} aligned with the internuclear vector). The sign of J([77]Se, ^{31}P) was identified as being negative through the spectral simulations (which depend on the relative signs of J([77]Se, ^{31}P) and R_{eff}([77]Se, ^{31}P)) and was corroborated with DFT computations (*vide infra*) and previous literature reports.[58]

The isotropic selenium chemical shifts increase in the presence of a halogen bond with iodine relative to those for the non-halogen-bonded Ph_3PSe (-257 and -242 ppm for its two crystallographic sites). The δ_{iso}([77]Se) values for compounds **1**, **2**, and **3** range from -140 ppm for site 2 of compound **3** to -220 ppm for site 2 in compound **1**. When the values of δ_{iso}([77]Se) are plotted as a function of their respective P=Se distances, a linear correlation is observed (Figure 6 (a)). An analogous trend was observed for the [77]Se chemical shifts of selenocyanate anions halogen-bonded with *p*- or *o*-DITFB, where the value of δ_{iso}([77]Se) increases in a halogen-bonded environment.[35] Furthermore, DFT calculations on a $(CH_3)_3P=Se{\cdots}ICF_3$ cluster model revealed the same trend; the δ_{iso}([77]Se) value increases when the P=Se bond length increases, *vide infra*. The anisotropy of the [77]Se chemical shift tensor does not conclusively differentiate between Ph_3PSe and the halogen-bonded compounds.

Chemical Shifts. DFT Computations and Correlation with Halogen Bond Geometry

DFT calculations of ^{31}P and ^{77}Se magnetic shielding tensors were performed on cluster models involving the molecules which are halogen-bonded; the numerical results are tabulated in the Supplementary Information. The X-ray crystal structure heavy-atom atomic coordinates (all atoms except hydrogen) were used for these models, shown in Figure 1. Computations using either the revPBE functional and the ZORA/TZP basis set (including scalar relativistic effects), as implemented in the ADF software,[63] or the TPSS functional and the 6-311G** basis set as implemented in Gaussian 09[64] were used. Further details are given in the Experimental Section.

In Figure 6(b,c) are plotted the calculated ^{77}Se isotropic chemical shift and chemical shift tensor components versus the experimental values. Even though the calculated values are larger than the experimental ones, the experimental trend is well-reproduced for δ_{iso}(^{77}Se) at both levels of theory; linear fits with correlation coefficients, R^2, of 0.9708 and 0.9950 are noted for the TPSS and revPBE functionals, respectively. The trends in the principal components of the ^{77}Se chemical shift tensor are reasonably well-reproduced, particularly in the case of the TPSS method and the δ_{33} component (see Figure 6(c)).

Generally, there are multiple factors which could contribute to the lack of a perfect correlation between the experimental and computed chemical shift tensor parameters. Firstly, cluster models do not allow for a full treatment of the effect of crystal packing on the computed NMR parameters. The gauge-including projector-augmented wave (GIPAW) DFT method[65] enables calculations using periodic boundary conditions; however, the volume of the unit cells (2392.2 Å^3 for **2** to 5085.9 Å^3 for **3**) of these compounds results in computational demands which are beyond our current capabilities. Additionally, several theoretical[66,67,68] reports describe the challenges in establishing the best ^{77}Se absolute shielding scale;[87] the selenium chemical shift range is over 3000 ppm and the shielding constants are subject to relativistic effects.[58,69]

The P=Se distance, $d_{P=Se}$, is different for each of the compounds studied here (Table 1). It is well known from the IUPAC definition that the distance R—X of the halogen bond donor tends to increase when involved in a halogen bond;[2] however, in this case the same type of change is also noted for the halogen bond acceptor, Y—Z (i.e., Se=P). As mentioned above, a plot of experimental $\delta_{iso}(^{77}Se)$ values vs $d_{P=Se}$ for the compounds studied herein shows a reasonable linear correlation, with increased values of $d_{P=Se}$ corresponding to increased chemical shifts (Figure 6(a)). Weak inverse correlations of $\delta_{iso}(^{31}P)$ with $d_{P=Se}$ are also noted (see SI).

This experimental observation was corroborated using ZORA calculations on the model halogen bonded complex $(CH_3)_3P=Se\cdots ICF_3$. The halogen bond distance ($d_{I\cdots Se}$) was varied systematically between 3.40 ($R_{XB} = 0.85$) and 3.66 Å ($R_{XB} = 0.92$) in 0.04 Å increments. These R_{XB} values reflect the range observed experimentally. As can be seen in Figure 6(d), as the halogen bonding interaction is weakened, the optimal value of $d_{P=Se}$ decreases. When the calculated values of $\delta_{iso}(^{77}Se)$ are plotted as a function of $d_{P=Se}$, a linear correlation ($R^2 = 0.9615$) in accord with that observed experimentally is obtained (see SI).

$J(^{77}Se,^{31}P)$ Coupling in Halogen Bonds. Correlation with Structure and DFT NLMO Analysis.

Shown in Figure 7(a) is a plot of the calculated $J(^{77}Se, ^{31}P)$ coupling constants versus the experimentally measured values. For the calculations, two different cluster models were used. The first model (blue squares) consists of the halogen bond donor and acceptor molecules as depicted in Figure 1. The second model (black circles) consists only of (arene)$_3$PSe molecules, omitting the halogen bond donor(s). By comparing the results of the two sets of revPBE calculations with the experimental data, one can assess the impact of the halogen bond to iodine on the values of $J(^{77}Se, ^{31}P)$. That is, are the values of $J(^{77}Se, ^{31}P)$ sensitive to the halogen

bonding interaction? When the two linear fits are compared, it is seen that inclusion of the halogen bond donor(s) in the model results in a slope closer to unity (0.714 vs 0.315) and an increased correlation coefficient (R^2 = 0.9719 vs 0.8761). This suggests that indeed the halogen bond to selenium is manifested in the value of $J(^{77}Se, {}^{31}P)$. Analysis of the analogous data obtained using the TPSS functional (data in SI) also shows improved slopes (0.652 vs 0.306) and correlation coefficients (0.9371 vs 0.8832) when the halogen bond donors are included in the models. The root-mean-squared deviation (RMSD) between the experimental and calculated data when the halogen bond donors are included is 37 Hz for the revPBE functional and 82 Hz for the TPSS functional.

As shown in Figure 7(c), experimentally the $J(^{77}Se, {}^{31}P)$ coupling magnitudes are observed to increase as the halogen bonds to selenium weaken. To account for multiple iodine halogen bond donors to a single selenium site, a cumulative R_{XB} value was used in this plot (i.e., R_{XB} = 1 - (1-R_{XB}(donor1)) - (1-R_{XB}(donor2)) - …). To further understand the origins of the variations in $J(^{77}Se,{}^{31}P)$ for halogen-bonded complexes, additional calculations were carried out, including a NLMO DFT study. This type of calculation allows one to analyze the contributions of key molecular orbitals to the J coupling.[50,52] Calculations on a $(CH_3)_3PSe\cdots ICF_3$ cluster model reproduce the experimental correlation between $J(^{77}Se, {}^{31}P)$ and R_{XB} (see Figure 7(d)).

An analysis of the largest NLMO contributions to the $J(^{77}Se,{}^{31}P)$ coupling values was conducted for the $(CH_3)_3PSe\cdots ICF_3$ cluster model as a function of the R_{XB} value. Three major contributions are seen to influence the J coupling value: a selenium lone pair orbital (~43%)), the bonding P=Se orbital (~38 %) and the phosphorus core orbital (~15%). Figure 7 (b) shows how the first two of these contributions vary as a function of the R_{XB} value; it is clear that the variations in the contribution from the selenium core orbital determine the overall trend. The

14

lower part of Figure 7(b) shows how the sum of the three most important contributions changes

with the value of R_{XB} (red triangles) and how the sum of all contributions follows the same trend

(turquoise circles).

Calculations for compounds **1**, **2**, and **3** demonstrate that the isotropic $J(^{77}Se,^{31}P)$ coupling

constant originates largely from the ZORA analogue of the Fermi-contact spin-dipolar

mechanism (~80%) with non-negligible contributions from the paramagnetic spin-orbit

mechanism (~20%). Shown in Figure 8 are the NLMOs resulting in the largest contributions to

the isotropic J coupling. (Note that only the three largest contributions are listed and for this

reason the sums differ from 100%.) For Ph$_3$PSe and for the halogen-bonded compounds, the

largest contribution to $J(^{77}Se,^{31}P)$ arises from the selenium lone pair orbital and its relative

contribution is about ~57 % except for in compound **2** (81.7 %) and site 2 in **3** (81.7 %), which

both have the smallest experimental J coupling values (-626(2) Hz, -641(25) Hz for **2** and site 2

in **3**, respectively), the longest P=Se bonds (2.1320 Å and 2.1252 Å for **2** and site 2 in **3**,

respectively), and the strongest halogen bonding interactions. The P=Se bonding orbital makes

the second largest contribution to the J coupling. The relative contributions are about 30 %,

except again for the sites having the strongest halogen bonds, **2** (-16.9 %) and site 2 in **3** (**-16.6**

%). Percentage contributions are negative if they are opposite in sign to the sum of all other

contributions and therefore serve to reduce the total value. Finally, another contribution to

$J(^{77}Se,^{31}P)$ arises from the phosphorus core orbital or selenium core orbital. The NLMO

contributions from the iodine lone pair are minor (~ 0.1 to 0.6 %; see SI).

Conclusions

A series of compounds featuring P=Se⋯I-C halogen bonds has been prepared and characterized by X-ray diffraction and ^{31}P, ^{77}Se, and ^{13}C solid-state NMR spectroscopy. Phosphorus and selenium chemical shift tensors as well as $J(^{77}Se,^{31}P)$ coupling constants have been measured and interpreted with the aid of density functional theory computations. Informed by a comparison with pure triphenylphosphine selenide, we draw the following conclusions:

1. [77]Se isotropic chemical shifts increase due to halogen bonding with iodine, and correlate with the P=Se distance which in turn correlates inversely with the reduced halogen bond distance parameter R_{XB};

2. $J(^{77}Se,^{31}P)$ coupling constants increase in magnitude as the selenium-iodine halogen bonds weaken;

3. computed $J(^{77}Se,^{31}P)$ coupling constants improve relative to the experimental values when the iodinated halogen bond acceptor is included in the structural model used for the calculations, suggesting that $J(^{77}Se,^{31}P)$ coupling constants are at least in part diagnostic of the halogen bond;

4. a natural localized molecular orbital analysis provides insight into the orbitals which contribute to $J(^{77}Se,^{31}P)$; for example, contributions from the selenium lone pair orbital tend to dominate both the magnitude and trends in $J(^{77}Se,^{31}P)$, with the selenium-phosphorus bonding orbital being the second-largest contributor.

To our knowledge, this study represents the first systematic experimental examination of J coupling constants within the halogen bond fragment R-X⋯Y-Z. It will be of interest in future work to examine J couplings across the halogen bond, e.g., $J(R, Y)$. The existence of such couplings and their value in understanding the halogen bond have been examined computationally for small model systems;[47] however, experimental SSNMR measurements are

likely to be challenging due to the NMR properties of the nuclei involved in typical halogen

bonds and the probable small magnitude of the coupling constants.

Experimental

Synthesis

Iodobenzene derivatives (p-$C_6F_4I_2$, o-$C_6F_4I_2$) and triphenylphosphine selenide (Ph_3PSe)

were purchased from Aldrich and used without further purification. sym-$C_6F_3I_3$ was acquired

from Alfa Aesar and used as received. Compounds **1** and **2** were prepared according to the

literature.[70] The syntheses of **1** and **2** were scaled to yield 150 to 200 mg of the desired product

for SSNMR studies. o- or p-DITFB (0.1295 g, 0.32 mmol) was mixed with Ph_3PSe (0.1100 g,

0.32 mmol) in a small vial and dissolved in a minimum amount of dichloromethane at room

temperature. The mixture was left to evaporate slowly, yielding **1** and **2**. Compound **3** was

prepared by dissolving equimolar amounts of Ph_3PSe (0.0787 g, 0.23 mmol) with sym-$C_6F_3I_3$

(0.1175 g, 0.23 mmol) in a minimum amount of dichloromethane. A vial containing the solution

was then left at room temperature until the desired compound crystallized, (Ph_3PSe)(sym-$C_6F_3I_3$)

(**3**). All samples were prepared at natural isotopic abundance.

Single-Crystal X-ray Crystallography

Data collection results for compounds **1**, **2**, and **3** represent the best data sets obtained in

several trials for each sample. The crystals were mounted on thin glass fibers using paraffin oil.

Mounted crystals were cooled by a stream of dry air to 200.15 K prior to data collection. Data

were collected on a Bruker AXS KAPPA single crystal diffractometer equipped with a sealed

Mo tube source (wavelength 0.71073 Å) and APEX II CCD detector. Raw data collection and processing were performed with the APEX II software package from BRUKER AXS.[71] Diffraction data for **1**, **2**, and **3** were collected with a sequence of 0.5° ω scans at 0, 120, and 240° in φ. Unit cell parameters for **1** were verified to be consistent with the literature.[70] Systematic absences in the diffraction data set and unit cell parameters were consistent with the monoclinic **P2$_1$/n** space group for compounds **2** and **3**. Solutions in centrosymmetric space groups for all compounds yielded chemically reasonable and computationally stable results of refinement. The structures were solved by direct methods, completed with difference Fourier synthesis, and refined with full-matrix least-squares procedures based on F^2. All hydrogen atoms were treated as idealized contributions. All scattering factors are contained in several versions of the SHELXTL program library, with the latest version used being 6.12.[72] Crystallographic data and selected data collection parameters are reported in Table 2.

Powder X-ray Diffraction

Sample purity and identity were verified by X-ray powder diffraction analysis. All experiments were carried out using a Rigaku Ultima IV instrument at room temperature (298 ± 1 K) with Cu Kα_1 radiation (λ = 1.54060 Å). All experiments were carried out with 2θ ranging between 5 and 50° in increments of 0.02° at a rate of 0.6° per minute. Simulations of patterns from single crystal results were generated using Mercury software available from the Cambridge Crystallographic Data Centre and were compared to those observed for bulk reaction products.

Solid-State NMR Spectroscopy

All compounds were ground into fine powders and packed in 4 mm o.d. zirconia rotors. Data were acquired at the University of Ottawa using either a 9.4 T ($\nu_L(^{13}C)$ = 100.6 MHz, $\nu_L(^{31}P)$ =

161.976 MHz, $\nu_L(^{77}Se)$ = 76.311 MHz) magnet equipped with a Bruker Avance III 400 console

and a 4 mm Bruker triple resonance MAS probe or a 11.75 T ($\nu_L(^{13}C)$ = 125.758 MHz, $\nu_L(^{31}P)$ =

202.456 MHz, $\nu_L(^{77}Se)$ = 95.382 MHz) Bruker Avance 500 wide bore spectrometer equipped

with a 4 mm triple resonance MAS probe.   Some data were also acquired at the National

Ultrahigh-Field NMR Facility for Solids in Ottawa using a 21.1 T ($\nu_L(^{77}Se)$ = 171.668 MHz)

standard-bore magnet equipped with a Bruker AVANCE II 900 console and a double-resonance

MAS probe.

Spectra for ^{13}C, ^{31}P, and ^{77}Se were collected under CP/MAS conditions[73] with proton

decoupling. Experimental setup and pulse calibration were performed using solid glycine for ^{13}C

($\delta_{iso}(^{13}C=O)$ = 176.4 ppm with respect to TMS),[74,75] solid diammonium selenate (($NH_4)_2SeO_4$)

for ^{77}Se (δ_{iso} = 1040.2 ppm with respect to $Se(CH_3)_2(l)$),[76] and ammonium dihydrogen phosphate

for ^{31}P ($NH_4H_2PO_4$, δ_{iso} = 0.81 ppm with respect to H_3PO_4 in 85% D_2O).[77]

^{13}C SSNMR. Recycle delays were 35, 10, and 15 s respectively for **1**, **2**, and **3**. The proton $\pi/2$

pulse and contact time were set to 3.25 or 3.50 µs and 2 ms, respectively, in all cases. MAS

frequencies varied between 8 and 10 kHz.

^{31}P SSNMR. ^{31}P SSNMR experiments used a recycle delay of 6 s at 9.4 T and 30 s at 11.75 T.

The proton $\pi/2$ pulse length was optimized to 2.50 or 3.00 µs at 9.4 T and 4.50 µs at 11.75 T.

The contact time was 5 ms and 2 ms at 9.4 and 11.75 T, respectively. MAS frequencies varied

between 2.1 kHz and 10 kHz.

^{77}Se SSNMR. For ^{77}Se NMR experiments, the recycle delays were 34 s, 20 s, and 30s for

compounds **1**, **2**, **3**, respectively. The ^1H $\pi/2$ pulse length used for the CP experiments was

typically 3.75 μs at 9.4 T. The proton $\pi/2$ pulse lengths used at 11.75 and 21.1 T were 2.8 and

4.0 μs, respectively. The contact time was typically 20 ms.

Spectra were simulated using WSOLIDS[78] and SIMPSON.[79] Additional experimental details

may be found in the SI.

Computational Details

Cluster models were generated using the X-ray crystal structures' atomic coordinates and

are depicted in Figure 1. The structure of Codding and Kerr[80] was used for Ph_3PSe. ^{31}P and ^{77}Se

magnetic shielding tensors were calculated with the Amsterdam Density Functional (ADF)

software[81][63] or Gaussian09[64] software. The positions of the hydrogen atoms in the models were

optimized prior to NMR calculations. For the DFT calculations performed with Gaussian09

software, the TPSS functional[82] and 6-311G** basis set were used.

For all calculations using ADF, scalar relativistic effects were included via the zeroth-

order regular approximation (ZORA).[83] All contributions to the **J** coupling tensors were

included in the calculations. Natural localized molecular orbital (NLMO) analyses were

performed with the NBO 5.0 code[84] in ADF[50,63] and were visualized with the program adfview.

The revised PBE[85] generalized gradient approximation (GGA) exchange-correlation functional

was used with the ZORA triple zeta basis set for magnetic shielding and **J** tensor calculations.

Additionally the meta-GGA TPSS functional was used for a second set of *J* coupling

calculations. These calculations were performed using the High-Performance Virtual Computing

Laboratory (HPCVL).

A simplified model was prepared for the calculations on site 2 of compound **3**. In this

model, the *sym*-$C_6F_3I_3$ molecules were replaced by CF_3I and the positions of all other atoms were

fixed while the new fluorine positions were optimized before proceeding to the magnetic shielding and J coupling calculations. Also, a systematic study was performed on a small cluster model of $(CH_3)_3PSe{\cdots}ICF_3$ were the $Se{\cdots}I$ distance was varied systematically by increments of 0.04 Å between 3.40 ($R_{XB} = 0.85$) and 3.66 Å ($R_{XB} = 0.92$). For each calculation, the model was geometry optimized while keeping the $Se{\cdots}I$ distance fixed. With the converged geometry, the J coupling calculation combined with the NLMO analysis was then performed, as well as the magnetic shielding tensor calculations. Note that the halogen bond geometry itself is not optimized computationally in any of the present calculations.

The computed magnetic shielding tensors were analyzed using the EFGShield program.[86] Magnetic shielding tensors were converted to chemical shift tensors using the following equation: $\delta_{ij} = \frac{\sigma_{ref} - \sigma_{ij}}{1 - \sigma_{ref}}$ (where σ_{ref} = 2069 ppm for selenium in $Se(CH_3)_2(l)$[87] and where σ_{ref} = 331.51 ppm for phosphorus in H_3PO_4 (85% D_2O)[88]). The ADF output files from the J coupling calculations were analyzed to select the NLMOs with large contributions to the isotropic J coupling constant. The sum of the Lewis and non-Lewis terms are reported for the largest contributions.

Supplementary Information Available

Additional experimental details; crystallographic information files (CCDC 987456-987457); PXRD diffractograms; images of the packing diagrams for the halogen-bonded compounds; additional NMR spectra; NLMO analysis.

Table 1. Selected halogen bond intermolecular contact distances and angles.[a]

compound		$d_{I—C}$ /Å	$d_{I\cdots Se}$ /Å	R_{XB}[b]	$\theta_{C—I\cdots Se}$ /°	$d_{P=Se}$ /Å	$\theta_{P=Se\cdots I}$ /°	$\theta_{I\cdots Se\cdots I}$ /°	R_{DD}[d] / Hz
Ph$_3$PSe		-	-	-	-	2.1080	-	-	995
		-	-	-	-	2.1074	-	-	996
1 (Ph$_3$PSe)(*p*-C$_6$F$_4$I$_2$)[c]	Site 1	2.092	3.4224	0.86	166.5	2.1070	112.6	-	997
	Site 2	2.082	3.4944	0.88	171.4	2.1270	113.0	126.0	969
		2.078	3.6841	0.93	154.9	-	88.9	-	
2 (Ph$_3$PSe)(*o*-C$_6$F$_4$I$_2$)	Site 1	2.0986	3.4014	0.85	175.2	2.1320	104.0	139.8	962
		2.1034	3.5863	0.90	174.7	-	91.9	-	
3 (Ph$_3$PSe)(*sym*-C$_6$F$_3$I$_3$)	Site 1	2.0949	3.5528	0.89	166.8	2.1190	104.6	-	980
	Site 2	2.0901	3.5027	0.88	162.5	2.1252	107.3	118.6	972
		2.0886	3.6024	0.91	159.2	-	91.3	-	
		2.0842	3.9227	0.99	159.7	-	155.3	-	

[a] See models in Figure 1. Experimental values determined by single-crystal X-ray crystallography.

[b] $R_{XB} = d_{X\cdots Y}/\Sigma d_{VdW}$, the ratio of the distance between the halogen (i.e., I) and the electron donor (i.e., Se) to the sum of their van der Waals radii (1.98 Å for I and 2.00 Å for Se).

[c] Arman *et al.*[70]

[d] ^{77}Se-^{31}P dipolar coupling constant, $R_{DD} = (\frac{\mu_o}{4\pi})(\frac{\gamma_I \gamma_S h}{4\pi^2})\langle r_{IS}^{-3}\rangle$, where μ_o is the permeability constant, γ_I and γ_S are the magnetogyric ratios of the coupled spins I and S (i.e., ^{31}P and ^{77}Se) and $\langle r_{IS}^{-3}\rangle$ is the motionally-averaged inverse cube of the distance between the coupled nuclei.

Table 2. Crystallographic Data and Selected Data Collection Parameters

compound	2	3
empirical formula	$C_{24}H_{15}F_4I_2PSe$	$C_{48}H_{30}F_6I_6P_2Se_2$
formula weight / g/mol	743.09	1701.98
crystal size/ mm	0.28 x 0.19 x 0.17	0.22 x 0.14 x 0.13
crystal system	monoclinic	monoclinic
space group	P $2_1/n$	P $2_1/n$
Z	4	4
a/ Å	13.7022(3)	28.1286(7)
b/Å	12.7689(3)	9.4276(3)
c/ Å	13.9386(3)	23.3606(7)
α/ °	90	90
β/ °	101.2140(10)	93.1692(16)
γ/ °	90	90
Volume / Å^3	2392.16(9)	5085.92(27)
calculated density/ Mg/m^3	2.063	2.223
absorption coefficient/ mm^{-1}	4.259	5.214
F(000)	1400	3152
Θ range for data collection/ °	1.91 to 28.33	1.764 to 30.535
limiting indices	-18 <= h <= 18,	-29 <= h <= 32,
	-17 <= k <= 17,	-13 <= k <= 13,
	-17 <= l <= 18	-33 <= l <= 32
reflections collected/unique	31024/5895	77460
R (int)	0.0187	0.0297
completeness to Θ = 28.32/ %	98.9	99.4
max and min transmission	0.5313 and 0.3818	0.550 and 0.393
data/restraints/parameters	5895/0/289	15250 /0 /577
goodness-of-fit on F^2	1.049	1.017
final R indices [I > 2α(I)]	R1 = 0.0164,	R1 = 0.0287
	wR2 = 0.0416	wR2 = 0.0641
R indices (all data)	R1 = 0.0179,	R1 = 0.0379
	wR2 = 0.0424	wR2 = 0.0681
largest diff peak/hole/ e· Å^{-3}	0.407 and -0.757	1.625 and -2.108

Table 3. Experimental ^{31}P CS tensor parameters.[a]

compound		δ_{iso} / ppm	Ω / ppm [b]	κ [b]
Ph$_3$PSe[c]	site 1	35.90	161	0.47
	site 2	41.90	144	0.39
1 (Ph$_3$PSe)(p-C$_6$F$_4$I$_2$)	site 1	34.25(0.10)	134(4)	0.53(0.10)
	site 2	34.25(0.10)	134(4)	0.53(0.10)
2 (Ph$_3$PSe)(o-C$_6$F$_4$I$_2$)	site 1	31.85(0.13)	112(2)	1.00(0.15)
3 (Ph$_3$PSe)(sym-C$_6$F$_3$I$_3$)	site 1	35.82(0.10)	133(3)	0.45(0.03)
	site 2	34.00(0.10)	112(2)	0.46(0.01)

[a] Error bounds are given in parentheses.

[b] Isotropic chemical shift: $\delta_{iso}=(\delta_{11} + \delta_{22} + \delta_{33})/3$; span: $\Omega \approx \delta_{11} - \delta_{33}$; skew: $\kappa = 3(\delta_{22} - \delta_{iso})/(\delta_{11} - \delta_{33})$, where $\delta_{11} \geq \delta_{22} \geq \delta_{33}$.

[c] Previously reported by Demko et $al.$[58] and Grossmann et $al.$[59]

Table 4. Experimental ^{77}Se CS tensor parameters and $J(^{77}$Se, ^{31}P) values.^{a}

	compound		δ_{iso} / ppm	Ω / ppm ^{b}	κ ^{b}	$J(^{77}$Se, ^{31}P) / Hz	R_{eff} / Hz^{d}
	Ph$_3$PSe^{c}	site 1	-257	221	-0.58	-733	695
		site 2	-242	247	-0.62	-736	696
1	(Ph$_3$PSe)(p-C$_6$F$_4$I$_2$)	site 1	-220	160(15)	1.0(0.2)	-725(25)	697
		site 2	-163	260(30)	0.2(0.2)	-663(38)	669
2	(Ph$_3$PSe)(o-C$_6$F$_4$I$_2$)	site 1	-158	170(5)	1.0(0.2)	-626(2)	729
3	(Ph$_3$PSe)(sym-C$_6$F$_3$I$_3$)	site 1	-188	350(20)	0.25(0.20)	-717(17)	680
		site 2	-140	250(15)	0.35(0.20)	-641(25)	672

^{a} Error bounds are given in parentheses. Errors in the isotropic chemical shifts are 1 ppm or less.

^{b} See footnote b of Table 3.

^{c} CS tensors and $J(^{77}$Se, ^{31}P) previously reported.[58,59]

^{d} See main text for further explanation.
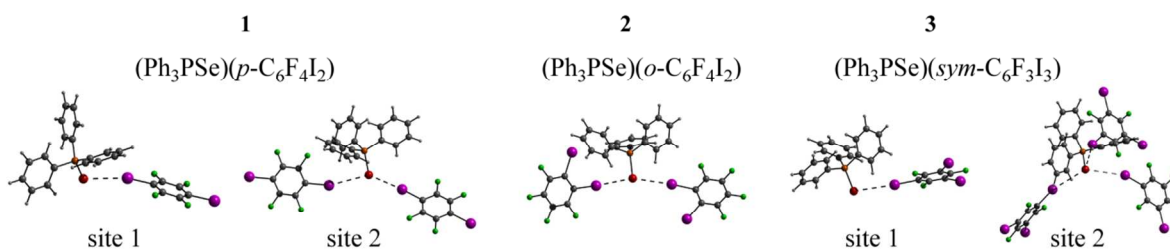
Figure 1. Local halogen bonding geometries for compounds **1**, **2**, and **3** studied in this work, from X-ray diffraction. See angles and bond lengths in Table 1. Compounds **1** and **3** have two crystallographically distinct selenium and phosphorus sites each. Each atom is colour-coded: selenium (red), phosphorus (orange), carbon (grey), iodine (purple), fluorine (green) and hydrogen (white).
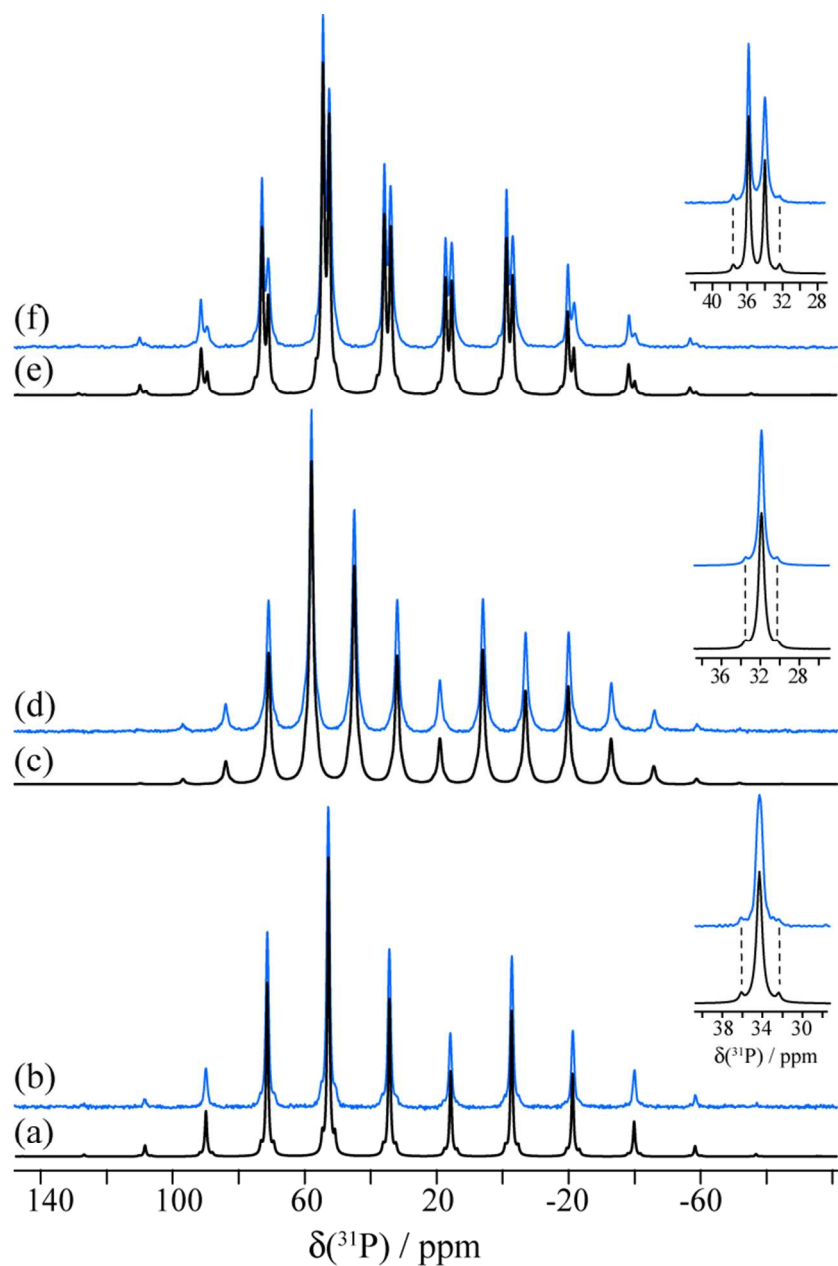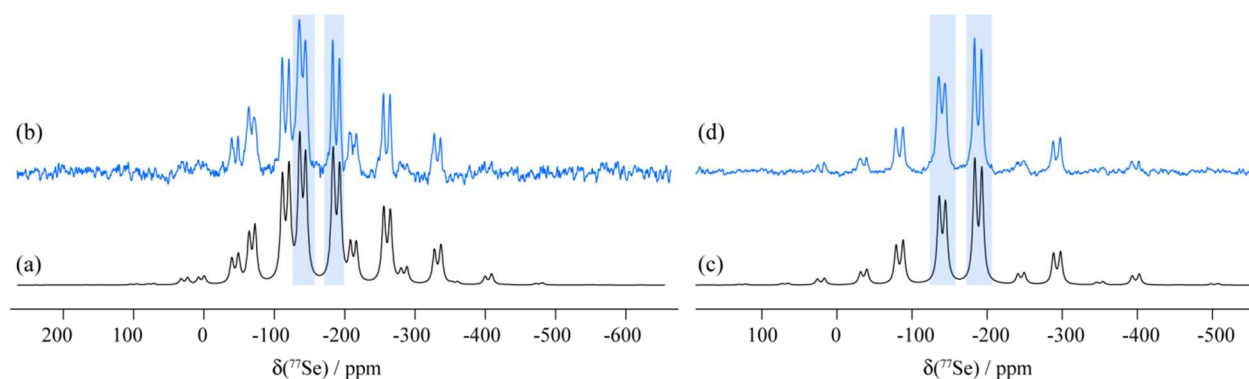
Figure 2. Experimental ^{31}P CP/MAS solid-state NMR spectra (blue) acquired at 9.4 T for (b) **1** (MAS 3 kHz), (d) **2** (MAS 2.1 kHz), and (f) **3** (MAS 3 kHz). Their respective simulated spectra are shown in black ((a), (c), (e)). Each inset shows the centreband and the ^{77}Se-^{31}P satellites due to *J* coupling (B_0 = 11.75 T). The top inset for compound **3** shows evidence of *J* coupling for both crystallographically distinct Se-P sites.
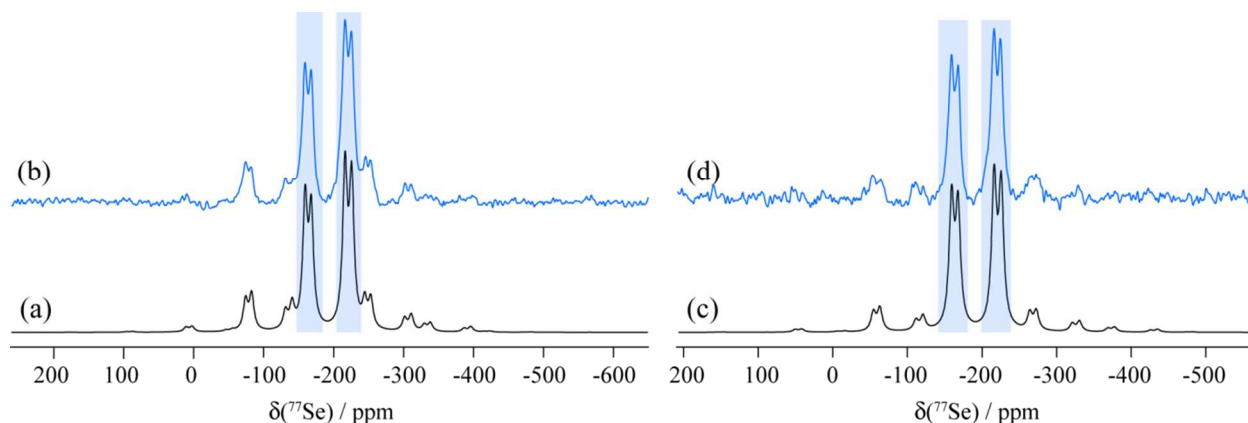
Figure 3. Experimental ^{77}Se CP/MAS solid-state NMR spectra acquired at 9.4 T with MAS rates of 6.5 kHz (b) and 8 kHz (d) for compound **1**. Simulations are shown in black. The centrebands for each of the two crystallographically distinct sites are highlighted in blue bars. Each of these is split into a doublet due to $J(^{77}$Se, ^{31}P) coupling.
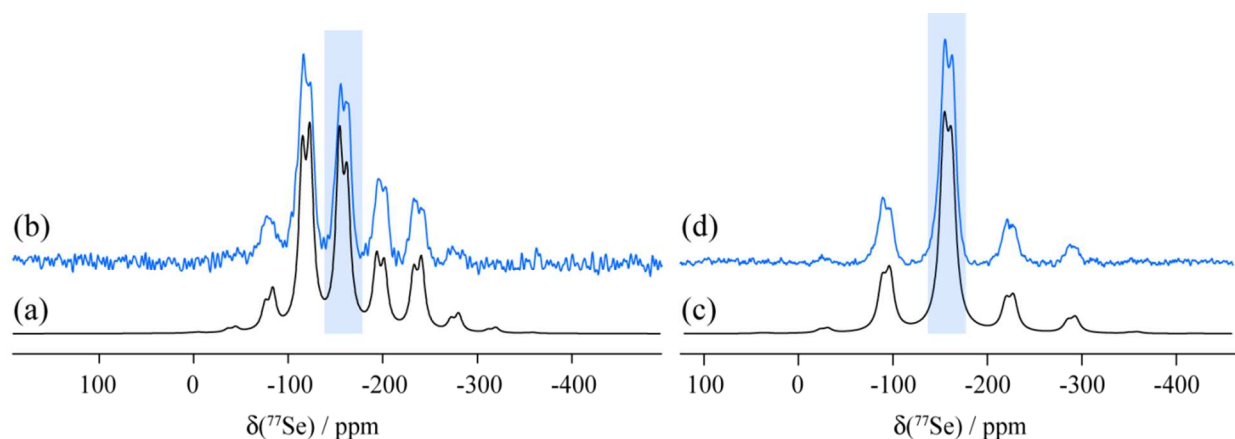

Figure 4. Experimental ^{77}Se CP/MAS solid-state NMR spectra acquired at 9.4 T with MAS rates of 3 kHz (b) and 5 kHz (d) for compound **2**. Simulations are shown in black ((a) and (c)). The centrebands, highlighted in blue bars, are split into doublets due to $J(^{77}$Se, ^{31}P) coupling. Small differences in the relative intensities of some of the peaks in the experimental and simulated spectra have been observed previously (see e.g,. Figures 6 and 9 of reference 58). Additionally, dipolar coupling to ^{19}F and ^{127}I may serve to further broaden and alter spectral intensities in the present work. From the crystal structure, the values of $R_{DD}(^{127}$I,^{77}Se) for the two shortest contacts are 118 and 101 Hz; the largest value of $R_{DD}(^{77}$Se,^{19}F) is 431 Hz.

Figure 5. Experimental ^{77}Se CP/MAS solid-state NMR spectra acquired at 9.4 T at a MAS rate of 5.5 kHz (b) and 8 kHz (d) for compound **3**. Simulations are shown in black ((a) and (c)). The centrebands, highlighted in blue bars, are split into doublets due to $J(^{77}$Se, ^{31}P) coupling. The relative intensities of sites 1 and 2 were adjusted to be ~1:1.2 for the best fit to experiment; we attribute this to differential cross-polarization efficiencies.
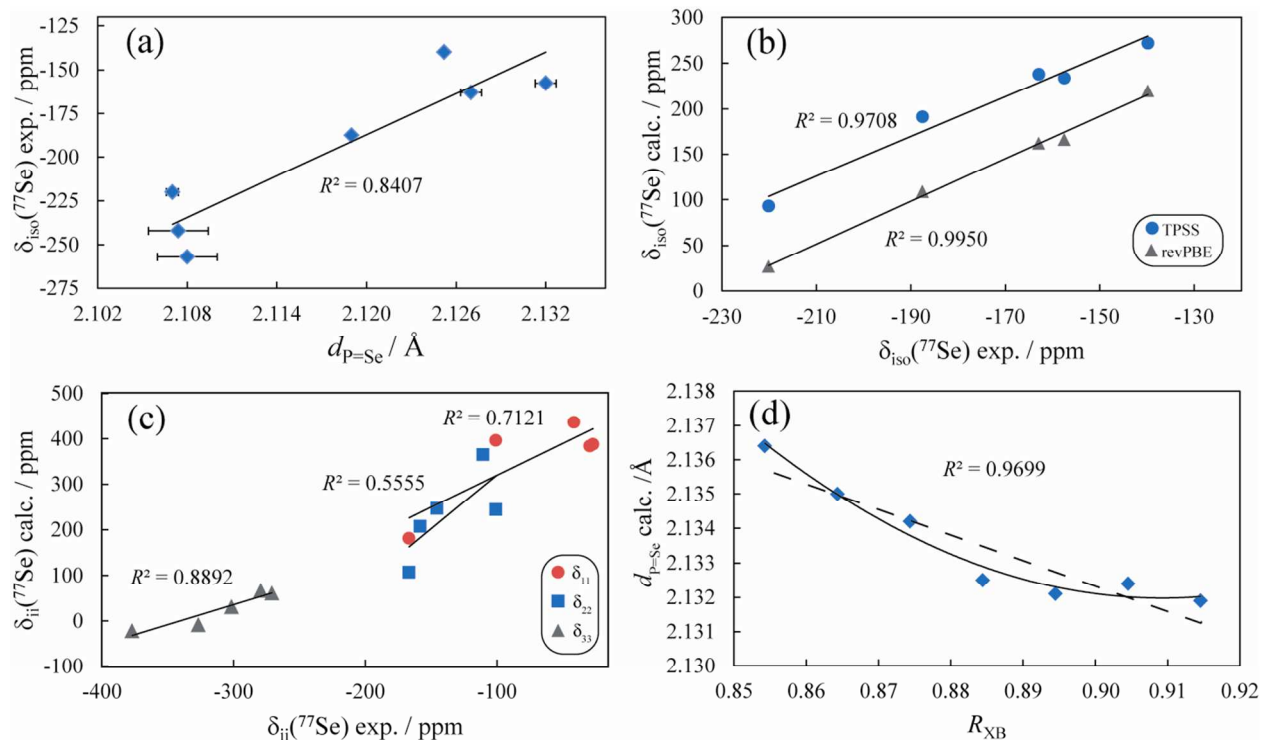
Figure 6. (a) Experimental $\delta_{iso}(^{77}Se)$ values as a function of the experimental P=Se bond lengths

for the compounds in Table 1 ($\delta_{iso}(^{77}Se)^{exp.} = 3924 d_{P=Se} - 8505$ ppm, $R^2 = 0.8407$). In (b) and (c)

are plots of calculated versus experimental chemical shift tensor parameters for selenium. Solid

lines represent the best linear fit: (b, TPSS) $\delta_{iso}^{calc.} = 2.1919\,\delta_{iso}^{exp.} + 586.08$ ppm, (b, revPBE)

$\delta_{iso}^{calc.} = 2.3368\,\delta_{iso}^{exp.} + 542.34$ ppm and (c, TPSS) $\delta_{11}^{calc.} = 1.4071\,\delta_{11}^{exp.} + 460.28$ ppm, $\delta_{22}^{calc.}$

$= 2.3579\,\delta_{22}^{exp.} + 555.75$ ppm and $\delta_{33}^{calc.} = 0.8816\,\delta_{33}^{exp.} + 300.06$ ppm. (d) Optimized $d_{P=Se}$

distances as function of R_{XB} for a cluster model comprised of $(CH_3)_3PSe\cdots ICF_3$ ($d_{P=Se}^{calc.} =$

$1.485(R_{XB})^2 - 2.701(R_{XB}) + 3.360$ ($R^2 = 0.9699$) or $d_{P=Se}^{calc.} = -0.0739 R_{XB} + 2.199$, $R^2 = 0.8642$).
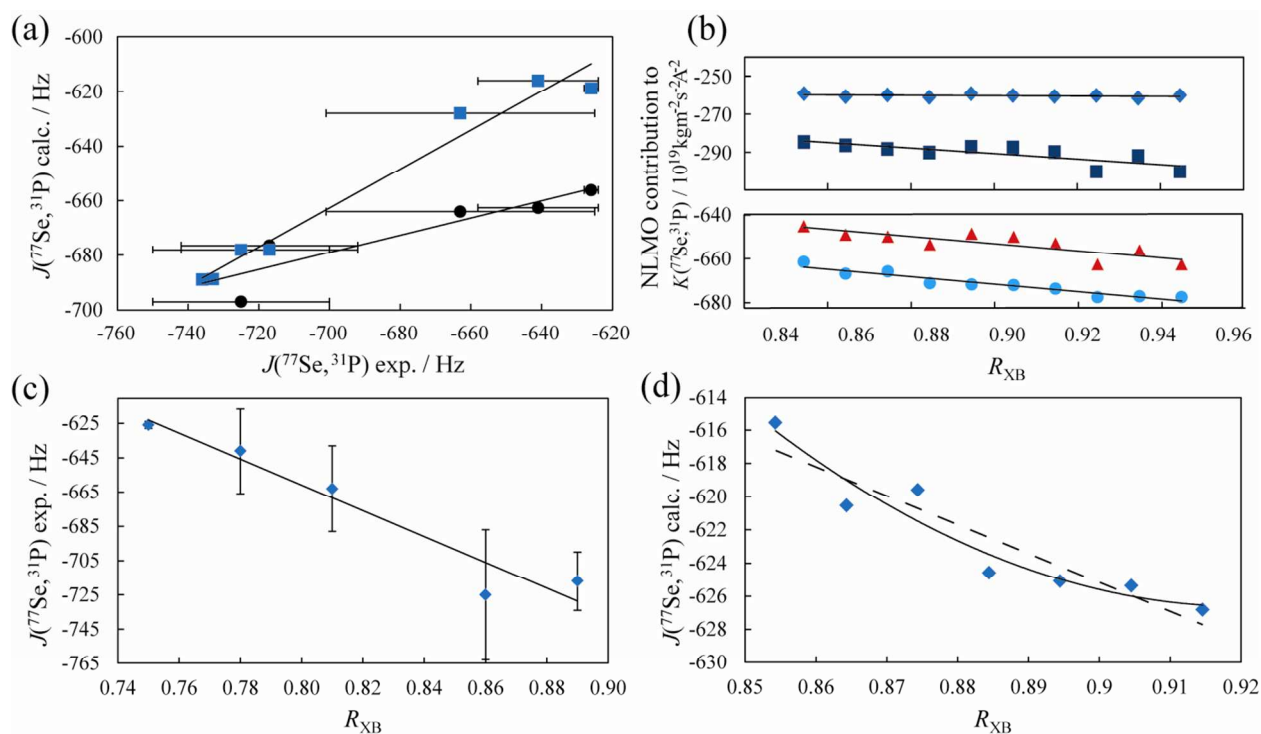
Figure 7. (a) Calculated versus experimental $J(^{77}Se, {}^{31}P)$ coupling constants for the compounds in Table 4 (revPBE ZORA/TZP). Two models were used: blue squares account for the model where the molecule of the halogen bonding acceptor and donor are included and the black circles omit all halogen bond acceptor(s) in the model. The solid lines are linear fits: (a, blue squares) $J(^{77}Se,{}^{31}P)^{calc.} = 0.714\ J(^{77}Se,{}^{31}P)^{exp.}$ - 163 Hz, $R^2 = 0.9719$, RMSD = 37 Hz, and (a, black circles) $J(^{77}Se,{}^{31}P)^{calc.} = 0.315\ J(^{77}Se,{}^{31}P)^{exp.}$ - 458 Hz, $R^2 = 0.8761$. (b) Plot of the sum of Lewis and non-Lewis largest NLMO contributions to $J(^{77}Se,{}^{31}P)$ as a function R_{XB} for the $(CH_3)_3PSe\cdots ICF_3$ cluster model (Top: blue diamonds represent the Se=P bonding orbital ($K = -9.81\ R_{XB} - 251.5$) and black squares represent the selenium lone pair orbital ($K = -144.9\ R_{XB} - 160.4$). Bottom: red triangles represent the sum of the contributions from the selenium lone pair orbital, the phosphorus lone pair orbital, and the Se=P bonding orbital ($K = -163.9\ R_{XB} - 505.6$) while the turquoise circles represent the total coupling including all other minor contributions ($K = -169.6\ R_{XB} - 518.9$)). (c) Experimental $J(^{77}Se, {}^{31}P)$ coupling constants for the compound in Table 4 as a function of R_{XB} ($J(^{77}Se,{}^{31}P)^{exp.} = -752.6\ R_{XB}$ - 58.77 Hz, $R^2 = 0.9304$). (d) Calculated $J(^{77}Se, {}^{31}P)$ coupling constants as a function of R_{XB} for the model compound $(CH_3)_3PSe\cdots ICF_3$ ($J(^{77}Se,{}^{31}P)^{calc.} = 2395.6\ (R_{XB})^2$ - 4411.5(R_{XB}) + 1404.3 Hz, $R^2 = 0.9699$ or $J(^{77}Se,{}^{31}P)^{calc.} = -174.15\ R_{RB}$ - 468.48 Hz, $R^2 = 0.8702$.) For the R_{XB} values in (c), when more than one halogen

bond donor interacts with the Se=P site, a cumulative value was used (R_{XB} = 1 - (1-R_{XB}(donor1)) - (1-R_{XB}(donor2)) - …).
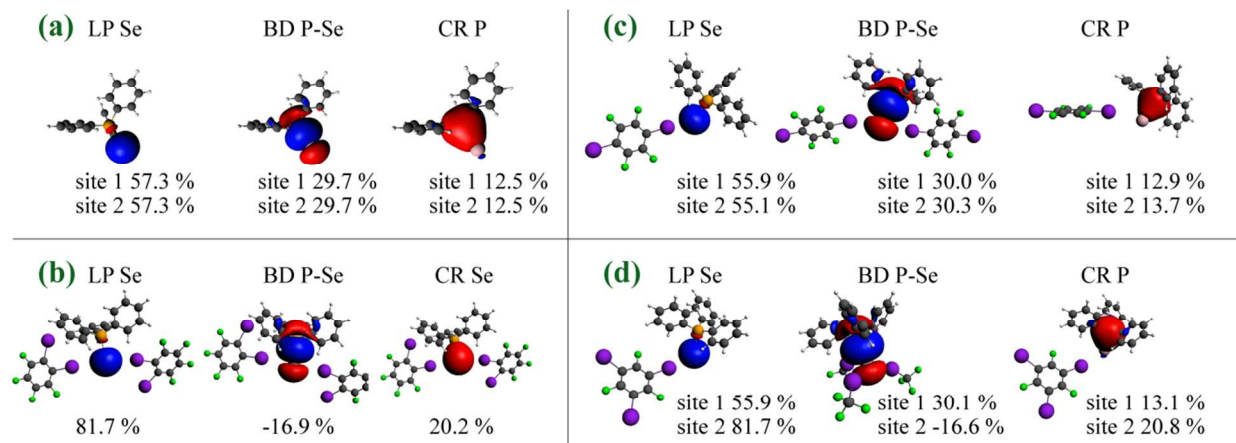
Figure 8. Selected NLMOs having the largest contributions to the isotropic $J(^{77}Se, ^{31}P)$ coupling values for halogen-bonded systems (**2** (b), **1** (c), **3** (d)) and Ph₃PSe (a). The percentages underneath the orbitals represent the contribution from the selenium lone pair (LP Se), the bonding orbital between P and Se (BD P-Se) orbital and the P core orbital (CR P) or Se core orbital (CR Se) to the isotropic J-coupling constant for each distinct selenium site. Note that the totals do not sum to 100% because only the largest contributions are shown.

References

[1] P. Metrangolo, G. Resnati (Eds.) *Halogen Bonding. Fundamentals and Applications* **2008**, Structure and Bonding, Volume 126, Springer: Heidelberg. Series editor D. M. P. Mingos.

[2] G. R. Desiraju, P. S. Ho, L. Kloo, A. C. Legon, R. Marquardt, P. Metrangolo, P. Politzer, G. Resnati, K. Rissanen, *Pure Appl. Chem.*, 2013, **85**, 1711.

[3] (a) F. Guthrie, *J. Chem. Soc.,* 1863, **16**, 239; (b) O. Hassel, *Science*, 1970, **170**, 497.

[4] (a) D. L. Bryce, *Chem. Int.*, 2012, **34**, 27; (b) J. Kemsley, *Chem. Eng. News*, 2012, August 27, 36.

[5] A. Priimagi, G. Cavallo, P. Metrangolo, G. Resnati, *Acc. Chem. Res.*, 2013, **46**, 2686.

[6] M. R. Scholfield, C. M. Vander Zanden, M. Carter, P. S. Ho, *Prot. Sci.*, 2013, **22**, 139.

[7] T. M. Beale, M. G. Chudzinski, M. G. Sarwar, M. S. Taylor, *Chem. Soc. Rev.*, 2013, **42**, 1667.

[8] Y. Lu, Y. Liu, Z. Xu, H. Li, H. Liu, W. Zhu, *Exp. Opin. Drug Discov.*, 2012, **7**, 375.

[9] M. Erdélyi, *Chem. Soc. Rev.*, 2012, **41**, 3547.

[10] M. Fourmigué, *Curr. Opin. Solid State Mater. Sci.*, 2009, **13**, 36.

[11] A. C. Legon, *Phys. Chem. Chem. Phys.*, 2010, **12**, 7736.

[12] P. Politzer, J. S. Murray, T. Clark, *Phys. Chem. Chem. Phys.*, 2010, **12**, 7748.

[13] K. E. Riley, P. Hobza, *Phys. Chem. Chem. Phys.*, 2013, **15**, 17742.

[14] K. E. Riley, J. S. Murray, J. Fanfrlik, J. Řezáč, R. J. Solá, M. C. Concha, F. M. Ramos, P. Politzer, *J. Mol. Model.*, 2013, **19**, 4651.

[15] K. E. Riley, P. Hobza, *J. Chem. Theory Comput.*, 2008, **4**, 232.

[16] T. Clark, M. Hennemann, J. S. Murray, P. Politzer, *J. Mol. Model.*, 2007, **13**, 291.

[17] P. Politzer, K. E. Riley, F. A. Bulat, J. S. Murray, *Comp. Theor. Chem.*, 2012, **998**, 2.

[18] P. Politzer, J. S. Murray, T. Clark, *Phys. Chem. Chem. Phys.*, 2013, **15**, 11178.

[19] A. R. Voth, F. A. Hays, P. S. Ho, *Proc. Natl. Acad. Sci. U. S. A.*, 2007, **104**, 6188.

[20] M. Carter, A. R. Voth, M. R. Scholfield, B. Rummel, L. C. Sowers, P. S. Ho, *Biochemistry*, 2013, **52**, 4891.

[21] G. Cavallo, P. Metrangolo, T. Pilati, G. Resnati, M. Sansotera, G. Terraneo, *Chem. Soc. Rev.*, 2010, **39**, 3772.

[22] L. C. Gilday, N. G. White, P. D. Beer, *Dalton Trans.*, 2012, **41**, 7092.

[23] M. G. Sarwar, B. Dragisic, E. Dimitrijevic, M. S. Taylor, *Chem. Eur. J.*, 2013, **19**, 2050.

[24] P. Metrangolo, Y. Carcenac, M. Lahtinen, T. Pilati, K. Rissanen, A. Vij, G. Resnati, *Science*, 2009, **323**, 1461.

[25] A. Peuronen, A. Valkonen, M. Kortelainen, K. Rissanen, M. Lahtinen, *Cryst. Growth Des.*, 2012, **12**, 4157.

[26] L. Meazza, J. A. Foster, K. Fucke, P. Metrangolo, G. Resnati, J. W. Steed, *Nat. Chem.*, 2013, **5**, 42.

[27] L. Gonzalez, N. Gimeno, R. M. Tejedor, V. Polo, M. B. Ros, S. Uriel, J. L. Serrano, *Chem. Mater.*, 2013, **25**, 4503.

[28] R. Gutzler, C. Fu, A. Dadvand, Y. Hua, J. M. MacLeod, F. Rosei, D. F. Perepichka, *Nanoscale*, 2012, **4**, 5965.

[29] P. Metrangolo, H. Neukirch, T. Pilati, G. Resnati, *Acc. Chem. Res.,* 2005, **38**, 386.

[30] F. Zordan, S. L. Purver, H. Adams, L. Brammer, *CrystEngComm*, 2005, **7**, 350.

[31] C. B. Aakeröy, S. Panikkattu, P. D. Chopade, J. Desper, *CrystEngComm*, 2013, **15**, 3125.

[32] C. B. Aakeröy, M. Fasulo, N. Schultheiss, J. Desper, C. Moore, *J. Am. Chem. Soc.*, 2007, **129**, 13772.

[33] A.-C. C. Carlsson, J. Gräfenstein, A. Budnjo, J. L. Laurila, J. Bergquist, A. Karim, R. Kleinmaier, U. Brath, M. Erdélyi, *J. Am. Chem. Soc.*, 2012, **134**, 5706.

[34] X. Q. Yan, X. R. Zhao, H. Wang, W. J. Jin, *J. Phys. Chem. B.*, 2014, **118**, 1080.

[35] J. Viger-Gravel, I. Korobkov, D. L. Bryce, *Cryst. Growth Des.*, 2011, **11**, 4984.

[36] J. Viger-Gravel, S. Leclerc, I. Korobkov, D. L. Bryce, *CrystEngComm*, 2013, **15**, 3168.

[37] R. J. Attrell, C. M. Widdifield, I. Korobkov, D. L. Bryce, *Cryst. Growth Des.*, 2012, **12**, 1641.

[38] C. M. Widdifield, G. Cavallo, G. A. Facey, T. Pilati, J. Lin, P. Metrangolo, G. Resnati, D. L. Bryce, *Chem. Eur. J.*, 2013, **19**, 11949.

[39] S. Grzesiek, F. Cordier, V. Jaravine, M. Barfield, *Prog. Nucl. Magn. Reson. Spectrosc.*, 2004, **45**, 275.

[40] A. J. Dingley, S. Grzesiek, *J. Am. Chem. Soc.*, 1998, **26**, 8293.

[41] S. P. Brown, M. Pérez-Torralba, D. Sanz, R. M. Claramunt, L. Emsley, *Chem. Commun.*, 2002, 1852.

[42] Y.-X. Wang, J. Jacob, F. Cordier, P. Wingfield, S. J. Stahl, S. Lee-Huang, D. Torchia, S. Grzesiek, A. Bax, *J. Biomol. NMR*, 1999, **14**, 181.

[43] H. Benedict, I. G. Shenderovich, O. L. Malkina, V. G. Malkin, G. S. Denisov, N. S. Golubev, H.-H. Limbach, *J. Am. Chem. Soc.*, 2000, **122**, 1979.

[44] N. S. Golubev, I. G. Shenderovich, S. N. Smirnov, G. S. Denisov, H.-H. Limbach, *Chem. Eur. J.*, 1999, **5**, 492.

[45] M. P. Ledbetter, G. Saielli, A. Bagno, N. Tran, M. V. Romalis, *Proc. Natl. Acad. Sci. U. S. A.*, 2012, **109**, 12393.

[46] M. J. Plevin, D. L. Bryce, J. Boisbouvier, *Nat. Chem.*, 2010, **2**, 466.

[47] J. E. Del Bene, I. Alkorta, J. Elguero, *J. Phys. Chem. A*, 2008, **112**, 7925.

[48] R. Garcia-Rodríguez, H. Liu, *J. Phys. Chem. A*, 2014, DOI :10.1021/jp411681f.

[49] P. A. W. Dean, M. K. Hughes, *Can. J. Chem.*, 1980, **58**, 180.

[50] J. Autschbach, *J. Chem. Phys.*, 2007, **127**, 124106.

51 A. J. Rossini, R. W. Mills, G. A. Briscoe, E. L. Norton, S. J. Geier, I. Hung, S. Zheng, J. Autschbach, R. W. Schurko, *J. Am. Chem. Soc.*, 2009, **131**, 3317.

52 S. Zheng, J. Autschbach, *Chem. Eur. J.*, 2011, **17**, 161.

53 A. Sutrisno, A. Y. H. Lo, J. A. Tang, J. L. Dutton, G. J. Farrar, P. J. Ragogna, S. Zheng, J. Autschbach, R. W. Schurko, *Can. J. Chem.*, 2009, **87**, 1546.

54 L. A. O'Dell, R. W. Schurko, K. J. Harris, J. Autschbach, C. I. Ratcliffe, *J. Am. Chem. Soc.*, 2011, **133**, 527.

55 (a) A. Bondi, *J. Phys. Chem.*, 1964, **68**, 441. (b) R. D. Shannon, *Acta Cryst.*, 1976, **A32**, 751.

56 (a) P. Pyykkö, A. Görling, N. Rösch, *Mol. Phys.*, 1987, **61**, 195; (b) M. Kaupp, O. L. Malkina, V. G. Malkin, *Chem. Phys. Lett.*, 1997, **265**, 55; (c) M. Kaupp, O. L. Malkina, V. G. Malkin, P. Pyykkö, *Chem. Eur. J.*, 1998, **4**, 118.

57 R. D. Chambers, *J. Chem. Soc. Perkin Trans. 1: Organic and Bio-Organic Chemistry*, 1996, **14**, 1659.

58 B. A. Demko, K. Eichele, R. E. Wasylishen, *J. Phys. Chem. A*, 2006, **110**, 13537.

59 G. Grossmann, M. J. Potrzebowski, U. Fleischer, K. Krüger, O. L. Malkina, W. Ciesielski, *Solid State Nucl. Magn. Reson.*, 1998, **13**, 71.

60 U. Haubenreisser, U. Sternberg, A.-R. Grimmer, *Mol. Phys.*, 1987, **60**, 151.

61 H. Bai, R. K. Harris, *J. Magn. Reson.*, 1992, **96**, 24.

62 D. L. Bryce, *Tensor Interplay*, *eMagRes,* 2008. DOI: 10.1002/9780470034590.emrstm1039

63 (a) G. te Velde, F. M. Bickelhaupt, S. J .A. van Gisbergen, C. Fonseca Guerra, E. J. Baerends, J. G. Snijders, T. Ziegler, *J. Comp. Chem.*, 2001, **22**, 931. (b) C. Fonseca Guerra, J. G. Snijders, G. te Velde and E. J. Baerends, *Theor. Chem. Acc.*, 1998, **99**, 391. (c) E. J. Baerends et al. Amsterdam Density Functional Software ADF2009.01 *SCM*; Theoretical Chemistry, Vrije Universiteit: Amsterdam, The Netherlands, http://www.scm.com/, 2010.

64 M. J. Frisch et al., Gaussian 09, rev. A.02; Gaussian, Inc.: Wallingford, CT, **2009**.

65 (a) C. J. Pickard, F. Mauri, *Phys. Rev. B*, 2001, **63**, 245101. (b) J. R. Yates, C. J. Pickard, F. Mauri, *Phys. Rev. B*, 2007, **76**, 024401. (c) M. Profeta, F. Mauri, C. J. Pickard, *J. Am. Chem. Soc.*, 2003, **125**, 541. (c) S. J. Clark, M. D. Segall, C. J. Pickard, P. J. Hasnip, M. I. J. Probert, K. Refson, M. C. Payne, *Z. Kristallogr.*, 2005, **220**, 567.

66 J. Jokisaari, P. Lazzeretti, P. Pyykkö, P. *Chem. Phys.* 1988, **123**, 339.

67 M. Bühl, W. Thiel, U. Fleischer, W. Kutzelnigg, *J. Phys. Chem.* 1995, **99**, 4000.

68 G. Schreckenbach, Y. Ruiz-Morales, T. Ziegler, *J. Chem. Phys.* 1996, **104**, 8605.

69 W. Nakanishi, S. Hayashi, Y. Katsura, M. Hada, *J. Phys. Chem. A*, 2011, **115**, 8721.

70 H. D. Arman, E. R. Rafferty, C. A. Bayse, W. T. Pennington *Cryst. Growth Des.,* 2012, **12**, 4315.

[71] Bruker AXS: Bruker Suite, version 2008/3, Bruker AXS Inc., Madison, WI, USA 2008.

[72] G. M. Sheldrick, *Acta Crystallogr.*, 2008, A**64**, 112.

[73] J. Schaefer, E. O. Stejskal, *J. Am. Chem. Soc.*, 1976, **98**, 1031.

[74] W. L. Earl, D. L. VanderHart, *J. Magn. Reson.*, 1982, **48**, 35.

[75] A. K. Jameson, C. J. Jameson, *Chem. Phys. Lett.*, 1987, **134**, 461.

[76] M. J. Collins, C. I. Ratcliffe, J. A. Ripmeester, *J. Magn. Reson.*, 1986, **68**, 172.

[77] D. L. Bryce, G. M. Bernard, M. Gee, M. D. Lumsden, K. Eichele, R. E. Wasylishen, *Can. J. Anal. Sci. Spectrosc.*, 2001, **46**, 46.

[78] WSolids1 ver. 1.20.21, K. Eichele, Universität Tübingen, 2013.

[79] M. Bak, J. T. Rasmussen, N. C. Nielsen, *J. Magn. Reson.*, 2000, **147**, 296.

[80] P. W. Codding, K. A. Kerr, *Acta. Cryst. B*, 1979, **35**, 1261.

[81] (a) G. Schreckenbach, T. Ziegler, J. Phys. Chem., 1995, **99**, 606. (b) S. K. Wolff, T. Ziegler, E. van Lenthe, E. J. Baerends, *J. Chem. Phys.*, 1999, **110**, 7689.

[82] J. M. Tao, J. P. Perdew, V. N. Staroverov, and G. E. Scuseria, *Phys. Rev. Lett.*, 2003, **91**, 146401.

[83] J. Autschbach, T. Ziegler, J. Chem. Phys., 2000, **113**, 936.

[84] E. D. Glendening, J. K. Badenhoop, A. E. Reed, J. E. Carpenter, J. A. Bohmann, C. M. Morales, F. Weinhold, NBO 5.0, Theoretical Chemistry Institute, University of Wisconsin, Madison, 2001; http://www.chem.wisc.edu/~nbo5

[85] (a) J. P. Perdew, K. Burke, M. Ernzerhof, *Phys. Rev. Lett.*, 1996, **77**, 3865. (b) J. P. Perdew, K. Burke, M. Ernzerhof, *Phys. Rev. Lett.*, 1997, **78**, 1396.

[86] S. Adiga, D. Aebi, D. L. Bryce, *Can. J. Chem.* 2007, **85**, 496.

[87] C. J. Jameson, A. K. Jameson, *Chem. Phys. Lett.*, 1987, **135**, 254.

[88] C. J. Jameson, A. DeDios, A. K. Jameson, *Chem. Phys. Lett.*, 1990, **167**, 575.